Soft Matter

Accepted Manuscript

ROYAL SOCIETY OF CHEMISTRY

www.rsc.org/softmatter

Flexibility and Protection by Design: Imbricated Hybrid Microstructures of Bio-inspired Armor

Stephan Rudykh[a], *Christine Ortiz*[b] *and Mary C. Boyce*[c]

[a] Department of Mechanical Engineering, Massachusetts Institute of Technology, Cambridge 02139–4307, USA
[b] Department of Materials Science and Engineering, Massachusetts Institute of Technology, Cambridge 02139–4307, USA
[c] School of Engineering and Applied Science, Columbia University, New York 10027, USA

Keywords: soft matter, bio-inspired armor, indentation, bending, layered materials, 3D printing

Inspired by the imbricated scale-tissue flexible armor of elasmoid fish, we design hybrid stiff plate/soft matrix material architectures and reveal their ability to provide protection against penetration while preserving flexibility. Indentation and bending tests on bio-inspired 3D-printed prototype materials show that both protection and flexibility are highly tunable by geometrical parameters of the microstructure (plate inclination angle and volume fraction). We show that penetration resistance can be amplified by a factor of 40, while flexibility decreases in less than 5 times. Different deformation resistance mechanisms are found to govern flexibility (inter-plate matrix shear) versus penetration resistance (localized plate bending) for this microstructural architecture which, in turn, enables separation of these functional requirements in the material design. These experiments identify the tradeoffs between these typically conflicting properties as well as the ability to design the most protective material architecture for a required flexibility, providing new design guidelines for enhanced flexible armor systems.

Many biological species develop effective dermal armor during evolution [1, 2]. These natural design principles [3] inspire development of synthetic light-weight flexible armor. In particular, the imbricated stiff-scale/soft-tissue dermal systems, present in elasmoid fish, provide an excellent combination of flexibility and protective properties. Moreover, the ability to vary geometric features of the scale-tissue microstructure enables tailoring the local protection and flexibility performance of the material, depending on the requirements in different regions of the body. Inspired by these biological materials, researchers have recently

begun to explore the mechanical performance of these systems. Meyers et al. [4] studied the microstructure of the scales of the Arapaima and performed penetration tests. Browning et al. [5] experimentally and numerically investigated the performance of bio-inspired composites under compression. These authors also employed the finite element method to study the mechanics of indentation in protective soft composite analogues [5]. Zhu and coauthors [6, 7] focused on the puncture resistance of scaled skin from striped bass (Morone saxatilis). Vernerey and Barthelat proposed a micromechanical model for flexural response of the scaled skin [11], and analyzed the response under compression, stretch, and bending loadings [12].

In this work, we focus on identifying and tailoring the multifunctional and seemingly competing performance requirements of *both* flexibility and protection (penetration resistance) of bio-inspired scale/matrix composites. To this end, we perform indentation tests for estimating protective properties resisting penetration events and three-point bending for estimating the flexibility of 3D-printed composites over a range of microstructural parameters. The experimental results reveal advantageous microstructured configurations which can be used for design and further optimization of the materials. In particular, we demonstrate the existence of composite microstructures for which protection properties can be significantly enhanced without sacrificing flexibility. These microstructural configurations are governed by the volume fraction and inclination angle of the scales, and the response of the materials can be tailored for the required performance. Thus, while the composite can resist penetration, flexibility is also achieved due to the different deformation mechanisms of each loading condition, including mechanisms of inter-plate matrix shear, plate rotation and plate bending. These mechanisms give rise to the combination of enhanced protection and flexibility.

Experiments: Exemplar prototypes of layered stiff plate/soft matrix composite materials are

fabricated using a multi-material 3D-printer Objet Connex500. We use two photo-sensitive polymeric materials, an acrylic-based photo-polymer, VeroWhite (VW), and a soft elastomeric material, TangoPlus (TP). The transparent soft matrix was printed in TP (Young's modulus *0.78* MPa), and the stiffer plates were printed in VW (Young's modulus *1.2* GPa). Schematics of the composite microstructure and experiments are shown in Figure 1. The total height of the specimens is $H = 10$ mm, the length is $L = 150$ mm and the out-of-plane depth is $z = 20$ mm; the thickness of the stiff plates is $t = 0.5$ mm; the heights of the lower homogenous layer and the upper scale-matrix composite layer are the same, namely, $h = 5$ mm (see Fig. 1a). Specimens are fabricated with a range in scale inclination angles relative to the substrate: $\Theta = 10°, 20°, 30°,$ and $45°$; the volume fraction of the stiff phase is $c = 0.1, 0.2, 0.3,$ and 0.4. Also, homogenous and bilayer specimens, with $c = 0.0$ and $1.0,$ are 3D-printed and tested.

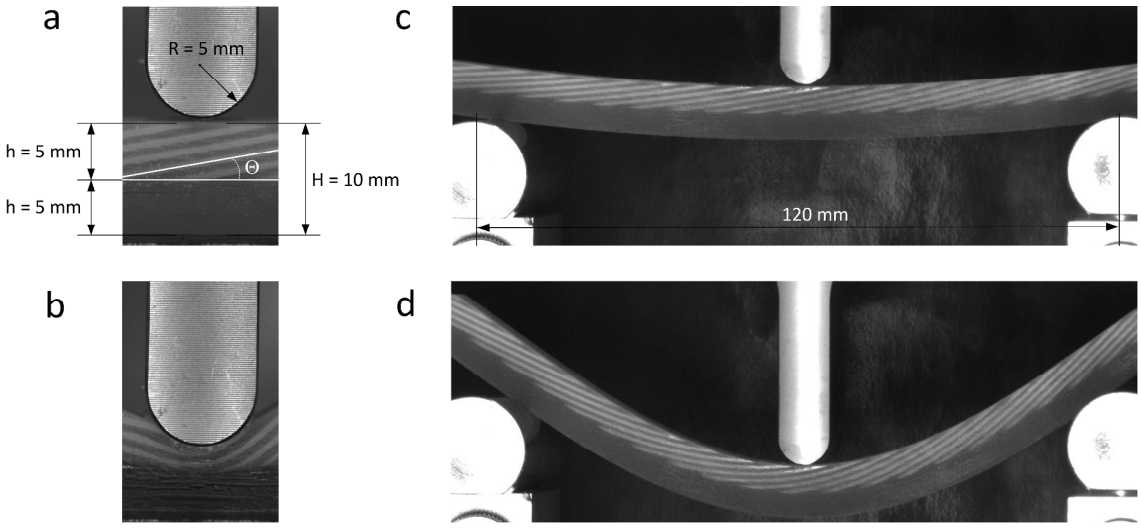

Figure 1: Schematics of the indentation and three-point bending tests. (a) – specimen before indentation; (b) – finite indentation. (c) – specimen at initial bending; (d) – finite bending of specimen.

To estimate the protective properties of the composites, we use indentation loading [8, 9] (see Fig. 1a and b). Flexibility was estimated by performing three-point bending tests (Fig. 1c and d), using a Zwick Mechanical Tester. The radius of the cylindrical indenter is *5* mm; the effects of the indenter size and shape are not specifically examined in this work; an indenter

radius of *R/t = 6*, *10*, *20*, *30* and *40* was shown in earlier works to induce similar response and underlying deformation mechanisms [8], when for *R/t* values of *0.1*, *1.0* and *10* the response was similar to the response observed for a sharp indenter [5]. The tests are performed quasi-statically with an indenter velocity of *0.1* mm/s, corresponding to a nominal engineering strain rate of *0.01*/s. Representative experiments are shown in Fig. 1.

Indentation tests: Figure 2 shows the responses to indentation for composites with $\Theta = 10°$ (a), *20°* (b), *30°* (c) and *45°* (d); and with *c = 0.0, 0.1, 0.2, 0.3, 0.4* and *1.0*, respectively. We plot normalized force $P = F/(\mu z H)$ as a function of normalized indentation depth, $\Delta = \delta / H$.

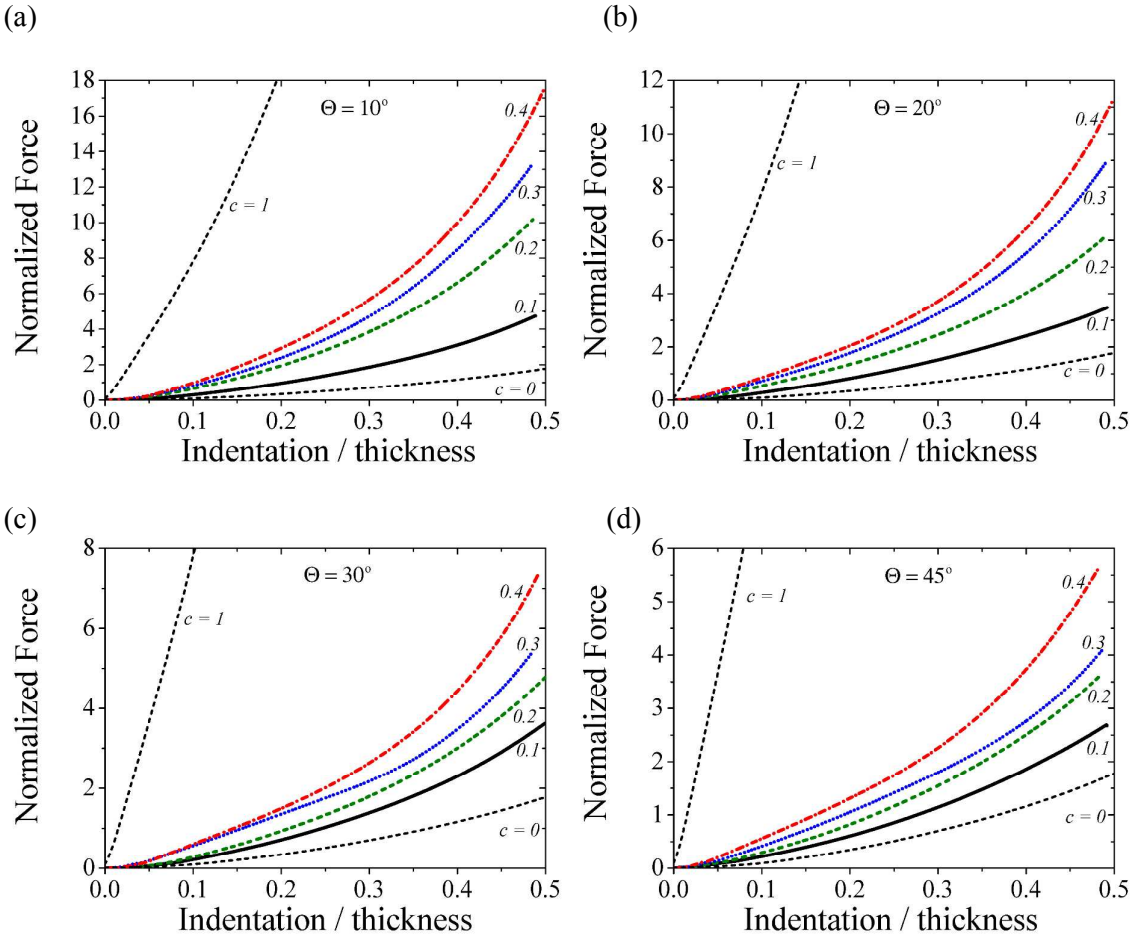

Figure 2: Force vs indentation depth for composites with $\Theta = 10°$ (a), *20°* (b), *30°* (c) and *45°*(d). The curves are for composites with *c = 0.0, 0.1, 0.2, 0.3, 0.4* and *1.0*, respectively.

The indentation force levels increase with an increase in stiff phase volume fraction. The

homogeneous case provides the lower limit of $c = 0.0$, while the stiffest response is observed for the bilayer composite, $c = 1.0$. An increase in inclination angle from $\Theta = 10°$ to $45°$ results in a decrease in the applied indentation force at the given indentation depth.

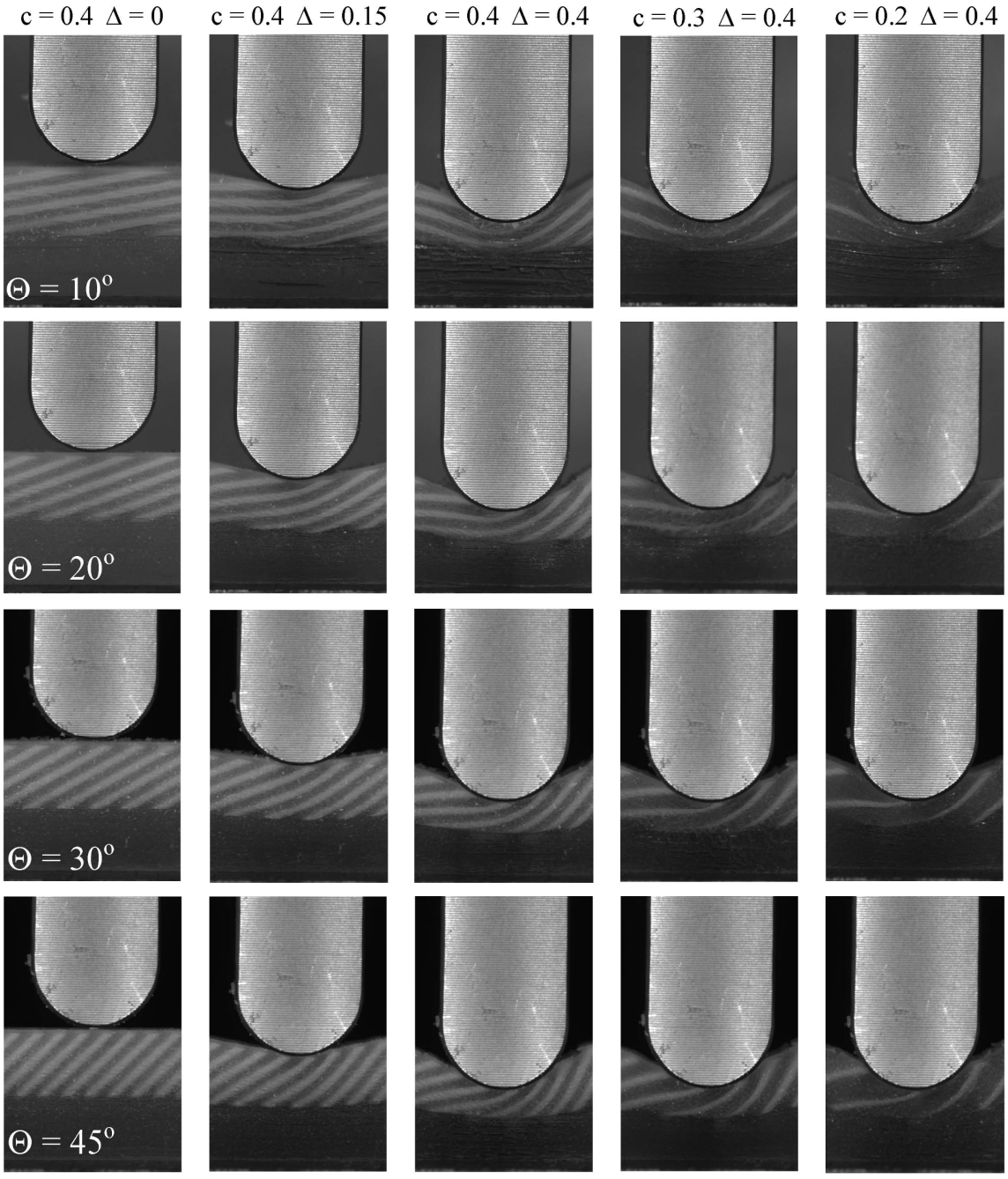

Figure 3: Illustration of deformation mechanisms in laminates. The first three columns are for laminates with $c = 0.4$ subjected to indentation depth $\Delta = 0.0, 0.15$, and 0.4(from left to right). Laminates subjected to $\Delta = 0.4$ are in column (4) and (5) for $c = 0.3$ and 0.2, respectively. The inclination angles are $\Theta = 10^o, 20^o, 30^o$, and 45^o in rows (1) to (4) – from top to bottom, respectively.

The different responses of the composites are governed by the underlying deformation

mechanisms, illustrated in Fig. 3. Figure 3 shows the microstructures of laminates of different inclination angle, Θ, and volume fraction, c, subjected to different levels of indentation depth Δ. Low indentation depths are primarily governed by inter-plate matrix shear, particularly for large inclination angles (Θ = *30* and *45* degrees), while significant localized plate bending is needed for penetration of small inclination angles even at low depths. These mechanisms were also observed in numerical simulations of similar layered structures [5, 8]. Matrix shearing is a lower resistance mode than plate bending and hence we observe lower penetration resistance for cases where matrix shear accommodates penetration – higher inclination angles more effectively resolve the applied load to inter-plate matrix shear and hence give lower penetration resistance. For greater depths, all inclination angles require plate bending to accommodate penetration; the number of plates and the extent of plate bending increase with increasing depth and also increase with an increase in volume fraction of plates and a decrease in inclination angle. Therefore, low inclination angles and high volume fractions offer the greatest penetration resistance, and penetration stiffness increases with increasing depth as shown in more detail next. We note that neither perforation nor other failures of the materials are observed.

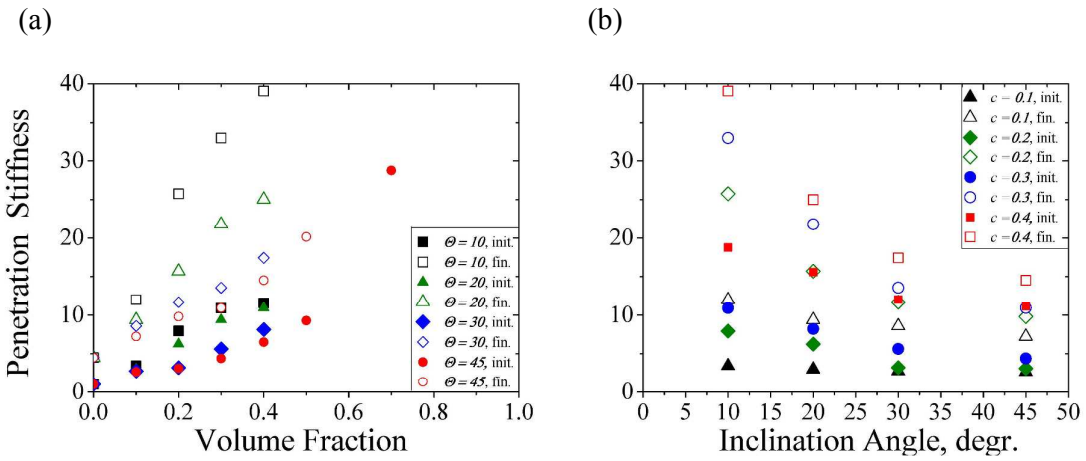

Figure 4: Relative penetration stiffness vs volume fraction (a) and inclination angle (b). The solid and hollow symbols are for initial and finite penetration stiffness, respectively.

The dependence of the material resistance against indentation is further shown by plotting the

relative *penetration stiffness* as a function of the volume fraction (Fig. 4a) and inclination angle (Fig. 4b). The penetration stiffness is defined here as the secant stiffness, $C^{(p)}(\Delta) = \frac{P(\Delta)}{\Delta}$, and the relative penetration stiffness is given as the value relative to the penetration stiffness of the homogeneous matrix, $c = 0.0$. Since the penetration stiffness changes with indentation depth, we plot the initial secant stiffness (measured at $\Delta = 0.01$) and the stiffness at finite indentation depth ($\Delta = 0.4$). The initial stiffness is presented by filled symbols, while the finite depth stiffness is denoted by hollow symbols. The finite depth stiffness is higher than the initial value reflecting the nonlinear behavior due to a combination of geometrical and material non-linearity. Both initial and finite stiffness increase with an increase in volume fraction, with stiffness increase more prominent for finite depth and small inclination angles for the reasons discussed above. For larger inclination angles, initially, an increase in volume fraction results only in a relatively small increase in stiffness. However, further increase in volume fraction leads to a rapid increase in stiffness due to the plate bending mechanism. The inclination angle has a strong effect on *finite* stiffness. Consistent with the previous observation, Fig. 4b shows that the penetration stiffness of the composites decreases with an increase in inclination angle. Thus, an increase in volume fraction or a decrease in inclination angle will increase the penetration stiffness. However, as shown next, these effects reduce the material flexibility.

(a) (b)

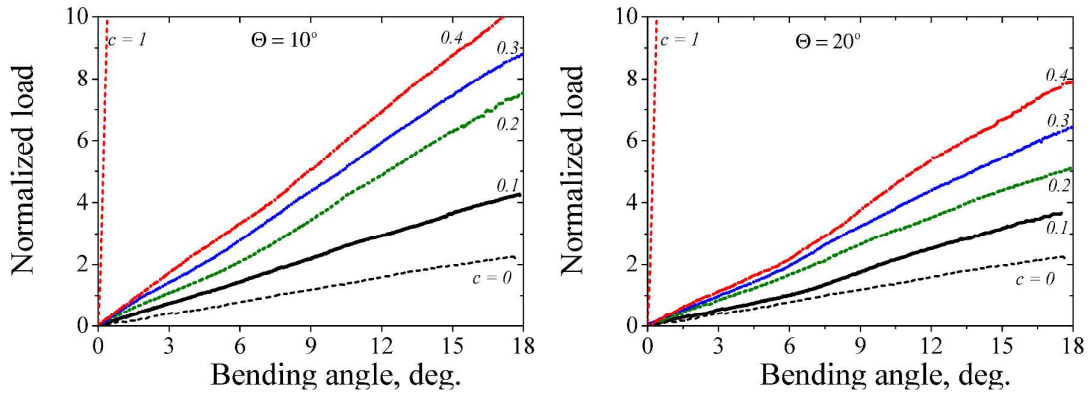

(c) (d)

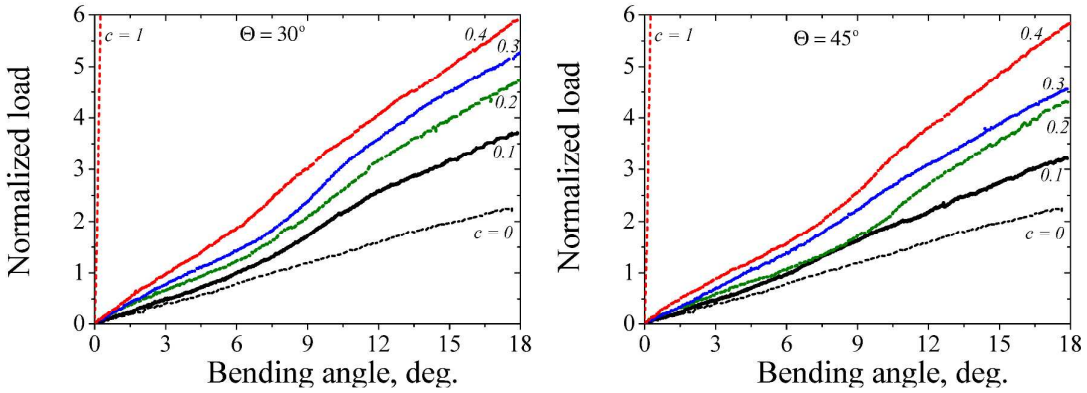

Figure 5: Normalized load vs bending angle for composites with $\Theta = 10°$ (a), $20°$ (b), $30°$ (c) and $45°$(d). The curves are for composites with $c = 0.1, 0.2, 0.3$ and 0.4; the upper and lower dashed curves are for $c = 1.0$ and homogeneous specimen.

Three point bending tests: Figure 5 shows the dependence of the normalized bending load on the bending angle for composites with $\Theta = 10°$ (a), $20°$ (b), $30°$ (c) and $45°$(d); and $c = 0.0, 0.1, 0.2, 0.3, 0.4$ and 1.0. The normalized bending load is defined as $M = \frac{F}{\mu z H}\frac{L_b}{t}$, where $L_b = 120\text{mm}$ is the distance between the supports shown in Fig. 1c. The bending angle is defined as $\varphi = \text{atan}(2\delta/L)$ [10]. Alternatively, a non-dimensional deflection can be used; the relation between these measures, as well as between corresponding stiffness is straight-forward. The composite flexibility decreases with an increase in volume fraction, as well as with a decrease in inclination angle. At smaller inclination angles, an increase in volume fraction results in a more pronounced increase in relative bending stiffness. The influence of volume fraction and inclination angle on the composite flexibility is further shown by plotting the relative bending stiffness as functions of these parameters in Fig. 6. Relative bending stiffness is taken as the bending stiffness of the composite (as measured by the secant stiffness $C^{(b)}(\varphi) = \frac{M(\varphi)}{\varphi}$) normalized to the bending stiffness of the homogeneous matrix. Similarly to the indentation test, we analyze both the initial (at $\varphi = 1°$) and finite (at $\varphi = 15°$) bending stiffness of the composites.

(a) (b)

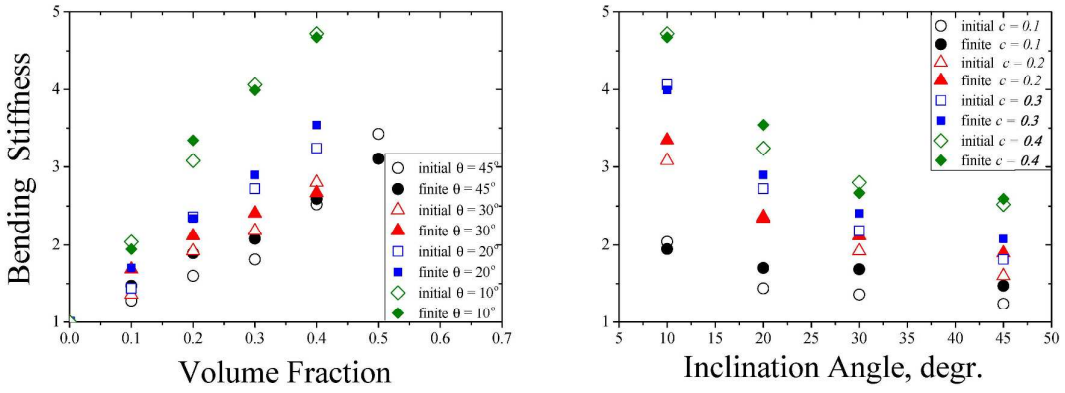

Figure 6: Relative bending stiffness vs volume fraction (a) and inclination angle (b). The solid and hollow symbols are for initial and finite bending stiffness, respectively.

We observe that, unlike the indentation tests, the bending behavior is nearly linear and stiffness does not change significantly with deformation. The composites show significant stiffening of the bending behavior with an increase in volume fraction; inclination angle provides a modest effect for high volume fractions and a relatively small influence for low volume fractions. Bending of the composite is accommodated by inter-plate matrix shearing which is dependent on plate volume fraction and inclination angle; local plate bending does not factor as a deformation mechanism during bending of these composites.

The fact that flexibility is governed by inter-plate matrix shearing and that the most effective penetration resistance is dominated by plate bending suggests that having these two different mechanisms possible in the same material structure offers the potential to achieve material designs which are protective yet flexible. Figure 7 shows the tradeoffs between flexibility and penetration resistance. In Figure 7a and b, we see bending stiffness as a function of penetration stiffness showing a general trend that an increase in protection is accompanied by a decrease in flexibility (increase in bending stiffness). However, closer inspection also shows that a given flexibility can be achieved with different penetration resistances - a relative bending stiffness of 2.5 can be obtained for designs that offer penetration resistances ranging between 10 and 22, and an initial penetration stiffness of 10 can be obtained for designs with

bending stiffness between 2.5 and 5. This clearly indicates that a different penetration resistance can be achieved for a given flexibility, or a different level of flexibility can be achieved for a different level of penetration resistance. To emphasize this idea we define a new metric which captures the contrasting combination of protection and flexibility, the *protecto-flexibility,* $\Psi = C^{(p)}/C^{(b)}$, taken as the ratio between the normalized indentation and normalized bending stiffness. The dependence of Ψ on the microstructural geometry of the composites is shown in Figure 7c and d, where *protecto-flexibility,* Ψ, is plotted vs volume fraction (c) and inclination angle (d). Note that initial *protecto-flexibility* does not change significantly with a change in volume fraction or inclination angle. However, the finite depth *protecto-flexibility* is very sensitive to changes in volume fraction and inclination angles. The composites with small and moderate inclination angles (Θ = *10°, 20°,* and *30°*) are characterized by a significant increase in *protecto-flexibility* with an increase in volume fraction. However, further increase in volume fraction leads to locking of the composite and significant loss of the flexibility, and, as a result, *protecto-flexibility* parameter drops at large volume fractions. We observe that volume fraction of approximately $c \sim 0.3$ is an optimal for achieving the best combination of penetration resistance and flexibility for most inclination angles and that smaller inclination angles of 10 degrees and 20 degrees provide the best combination of properties (for the initial Ψ, we see that 20 degrees provides higher Ψ than 20 degrees but at finite deformations, 10 degrees is preferable).

These results are presented for a fixed contrast in stiffness of the composite phases, namely $\sim$ *1,500*; although the influence of the contrast is not studied in this work in detail, it is possible that the stiff plate bending mechanisms would increase with a decrease in the stiffness ratio, while the stiff plate rotation based mechanism would become more prominent with an increase in the stiffness contrast.

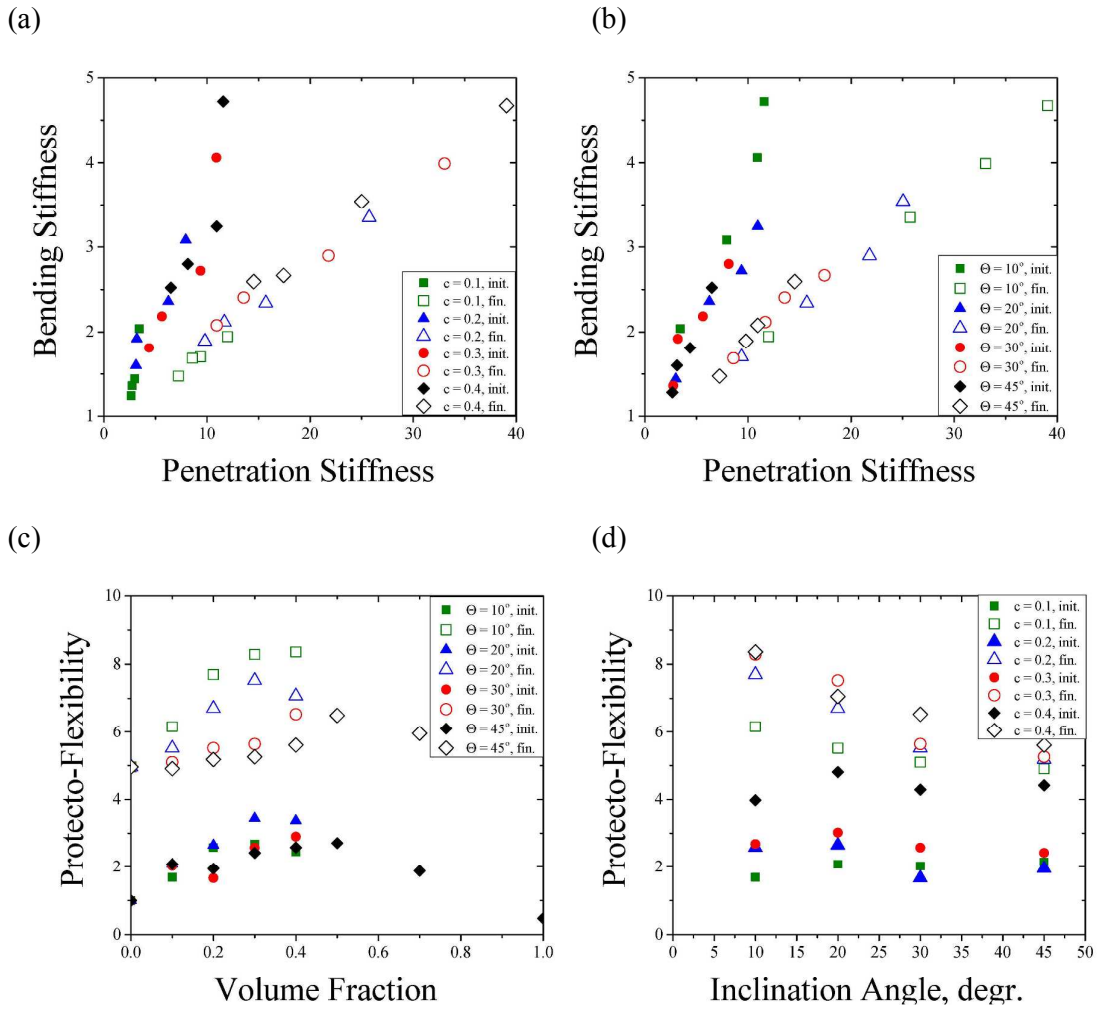

Figure 7: Relative bending stiffness vs relative penetration stiffness (a) and (b). Normalized indentation-to-bending stiffness ratio (protecto-flexibility) vs volume fraction (c) and inclination angle (d). The solid and hollow symbols are for initial and finite stiffness ratios, respectively.

Summary: We introduced a new metric for material performance that incorporates the conflicting performance requirements of penetration resistance and flexibility in one parameter, namely *protecto-flexibility*, and further analyzed the role of microstructural parameters in this integrated measure of competing material performance requirements. Our findings provide new guidelines for developing simple material architectures that retain flexibility while offering protection with highly tunable properties (i.e., both penetration resistance and flexibility). The tailored performance of the protective system (that can be

tuned according to the required movements at different regions of the body) draws the remarkable abilities from the microstructural geometry, which defines the micromechanical mechanisms active in response to loadings. The ability for a given microstructure to offer different deformation resistance mechanisms in different loading conditions is key to achieving the multifunctional design – the imbricated stiff plate/soft matrix provides a compliant matrix shearing deformation mechanism for flexibility and a highly resistance plate bending mechanisms to resist penetration. Careful selection of microstructural parameters can provide designs optimized to grant protection against penetration while preserving flexibility.

Acknowledgements
This research was supported by the U.S. Army Research Office through the MIT Institute for Soldier Nanotechnologies under contract W911NF-13-D-0001. CO gratefully acknowledges the support of the National Security Science and Engineering Faculty Fellowship Program (N00244-09-1-0064). SR acknowledges the support of Taub Foundation through the Horev Fellowship – Leaders in Science and Technology.

References

[1] Bruet, B., Song, J., Boyce, M. & Ortiz, C. (2008) Materials design principles of ancient fish armour. *Nature Mater.*, 7, 748–756.

[2]Connors, M., Ehrlich, H., Hog, M., Godeffroy, C., Araya, S., Kallai, I., Gazit, D., Boyce, M. & Ortiz, C. (2012) Three-dimensional structure of the shell plate assembly of the chiton tonicella marmorea and its biomechanical consequences. *J. Struct. Biol.*, 177, 314–328.

[3] Yang, W., Chen, I. H., Gludovatz, B., Zimmermann, E. A., Ritchie, R. O. & Meyers, M. A. (2013) Natural flexible dermal armor. *Adv. Mater.*, 25, 31–48.

[4] Meyers, M., Lin, Y., Olevsky, E. & Chen, P.-Y. (2012) Battle in the amazon: arapaima versus piranha. *Adv. Eng. Mater.*, 14, B279–B288.

[5] Browning, A., Ortiz, C. & Boyce, M. (2013) Mechanics of composite elasmoid fish scale assemblies and their bioinspired analogues. *J. Mech. Behav. Biomed. Mater.*, 19, 75–86.

[6] Zhu, D., Ortega, C., Motamedi, R., Szewciw, L., Vernerey, F. & Barthelat, F. (2012) Structure and mechanical performance of a 'modern' fish scale. *Adv. Eng. Mater*., 14, B185–B194.

[7] Zhu, D., Szewciw, L., Vernerey, F. & Barthelat, F. (2013) Puncture resistance of the scaled skin from striped bass: Collective mechanisms and inspiration for new flexible armor designs. *J. Mech. Behav. Biomed. Mater.*, 24, 30–40.

[8] Rudykh, S. and Boyce, M. C. (2014) Transforming Small Localized Loading into Large Rotational Motion in Soft Anisotropically-Structured Materials , *Adv. Eng. Mater*., 15, (11), 1311–1317 .

[9] S. Rudykh and M.C. Boyce (MIT) *USA 61/881022*, (2013).

[10] Rudykh, S. and Boyce, M. C. (2014), Analysis of elasmoid fish imbricated layered scale-tissue systems and their bio-inspired analogues at finite strains and bending. *IMA J. Appl. Math.*, 79, 830–847.

[11] Vernerey, F. J. and Bartelat, F. (2010). On the Mechanics of Fish-Scale Structures. *International Journal of Solids and Structures*, 47(17), 2268–2275.

[12] Vernerey, F.J. and Barthelat, F. (2014) Skin and scales of teleost fish: simple structure but high performance and multiple functions, *Journal of the Mechanics and Physics of Solids*, 68, 66-76.